RSC Advances

PAPER

View Article Online
View Journal | View Issue

Cite this: *RSC Adv.*, 2017, **7**, 24616

Hydrothermal synthesis and formation mechanism of the anatase nanocrystals with co-exposed high-energy {001}, {010} and [111]-facets for enhanced photocatalytic performance†

Xianjun Niu,[a] Yi-en Du,*[abc] Yufang Liu,[a] Hongxue Qi,[a] Jing An,[a] Xiaojing Yang *[b] and Qi Feng [c]

Truncated tetragonal bipyramid anatase TiO_2 nanocrystals enclosed by {001}, {010} and {101} facets, and tetragonal cuboid anatase TiO_2 nanocrystals with co-exposed [111]- and {101} facets were hydrothermally synthesized by using the H^+-form of the tetratitanate $H_2Ti_4O_9$ as the precursor and HF and H_2O_2 as the capping agent and solvent, respectively. The as-prepared anatase TiO_2 nanocrystals were characterized by X-ray diffraction (XRD), scanning electron microscopy (SEM), transmission electron microscopy (TEM) and high-resolution transmission electron microscopy (HRTEM), selected-area electron diffraction (SAED) and nitrogen adsorption/desorption measurements. The transformation from the layered structure of tetratitanate HTO to anatase TiO_2 nanocrystals may experience two types of reactions including *in situ* topotactic transformation reaction by splitting the Ti–O–Ti bonds of the corner-shared by two TiO_6 octahedra along the [010]-direction of the HTO, and the dissolution–recrystallisation reaction along various crystal planes of the zigzag ribbon-like anatase crystal during the hydrothermal reaction process. Furthermore, the photocatalytic activities of the as-prepared anatase nanocrystals were evaluated by the photocatalytic degradation of methylene blue under UV-light irradiation at room temperature in air. Truncated tetragonal bipyramid and cuboid coexistence of anatase TiO_2 nanocrystals with a large percentage of co-exposed high-energy {001}, {010} and [111]-facets exhibit high surface photocatalytic activities for the degradation amount of MB per unit surface area of catalyst (mg (MB) per m^2 (TiO_2 surface area)), which can be explained by the cooperative mechanism of the surface atomic structure and surface electronic structure of the different facets.

Received 31st March 2017
Accepted 28th April 2017

DOI: 10.1039/c7ra03707d

rsc.li/rsc-advances

1. Introduction

Titanium dioxide (TiO_2) crystals with tailored facets have attracted intensive interest in the last few years, not only because of their extensive applications in dye-sensitized solar cells,[1] photocatalytic degradation of organic pollutants,[2,3] gas sensors,[4] lithium-ion batteries,[5] and other related fields, but also because of their relatively high photocatalytic activity, long-term stability, nontoxicity and low cost.[6] Triggered by Wen's first report the preparation of anatase TiO_2 nanocrystals enclosed by dominant {010} facets,[7] tremendous efforts have been made to synthesize diverse TiO_2 nanocrystals with exposed high-energy or reactive facets. For anatase TiO_2, the order of average surface energies (γ) is $\gamma_{\{111\}}$ (1.61 J m^{-2}) > $\gamma_{\{110\}}$ (1.09 J m^{-2}) > $\gamma_{\{001\}}$ (0.90 J m^{-2}) > $\gamma_{\{010\}}$ (0.53 J m^{-2}) > $\gamma_{\{101\}}$ (0.44 J m^{-2}).[8,9] Unfortunately, surfaces with high-energies often decrease rapidly during the crystal growth process so as to reduce the surface energy.[10] According to the Wulff construction, the equilibrium shape of an anatase TiO_2 crystal can be theoretically constructed as a slightly truncated tetragonal bipyramid enclosed by eight equivalent {101} facets (more than 94%) on the lateral surfaces and two equivalent {001} facets on the top/bottom surfaces.[11] Since the {101} facets are quite unreactive, the most available anatase is dominated by energetically stable {101} facets, rather than the much more reactive {111}, {110}, {001}, or {010} facets. Therefore, constructing anatase TiO_2 with controllable highly active facets still remains a challenge.

[a]*School of Chemistry & Chemical Engineering, Jinzhong University, Jinzhong, Shanxi, 030619, P. R. China. E-mail: duyien124@163.com*

[b]*Beijing Key Laboratory of Energy Conversion and Storage Materials, College of Chemistry, Beijing Normal University, Beijing, 100875, China. E-mail: yang.xiaojing@bnu.edu.cn*

[c]*Department of Advanced Materials Science, Faculty of Engineering, Kagawa University, 2217-20 Hayashi-cho, Takamatsu-shi, 761-0396, Japan*

† Electronic supplementary information (ESI) available: Crystal phase, morphology, exposed facet, crystal size, and surface area for TiO_2 nanocrystals, UV-visible absorption spectra changes of methylene blue solution as a function of irradiation time in the presence of (a) P25-TiO_2, (b) T150-TiO_2, (c) T170-TiO_2, (d) T180-TiO_2 and (e) absence of TiO_2 nanocrystals catalyst. See DOI: 10.1039/c7ra03707d

Since the pioneering work by Wen and co-workers on the synthesis of anatase TiO_2 nanocrystals with large percentages of {010} facets by using $[Ti_{1.73}O_4]^{1.07-}$ nanosheets as the precursor,[7] there has been remarkable interest in the controlled synthesis of anatase crystals with high reactive facets, such as {010}, {001}, and {110} facets. For example, Yang and co-workers synthesized the truncated anatase bipyramids with different percentages of {001} facets (35–47%) and {101} facets by using $TiCl_4$ aqueous solution as the precursor and HF as the crystallographic controlling agent under hydrothermal conditions.[10] After that, by use of similar synthetic strategies, anatase TiO_2 nanosheets with dominant {001} facets (64%) and minor {101} facets have been prepared, which exhibited superior photoreactivity in degradation of organic pollutant, compared to the benchmark P25-TiO_2.[12] Wu and co-workers achieved the truncated tetragonal bipyramids with coexisting {001} and {101} facets containing a hole on the squared planer crystal facet, which showed higher photocatalytic activity for the photodegradation of rhodamine B in water.[13] Furthermore, {001}-facet exposed TiO_2 microspheres were synthesized by hydrothermal treatment of a thermal sprayed TiN/Ti coating with HF aqueous solution containing chromium powders, which led to a significantly enhanced solar absorption.[14] Liu and co-workers reported the anatase TiO_2 single crystals with co-exposed {001} and {101} facets, together with minor {110} facets were synthesized by using a hydrothermal technique in the presence of H_2O_2 and HF, and demonstrated their photocatalytic activities.[9] Single anatase crystals with co-exposed {001}, {010}, and {101} facets, together with minor {110} facets have been prepared by tuning the Ti/F ratio in the synthetic mixture. Recently, enlarging {110} exposed facets of anatase TiO_2 microcrystals were synthesized by a one-step hydrothermal methods, in the present of HF, H_2O_2 and $TiCl_3$.[15] Rhombic-shaped anatase TiO_2 nanocrystals with co-exposed {010} and {101} facets have been synthesized by using a facile nonaqueous synthetic route, which exhibited conspicuous photocatalytic activity.[16] Anatase TiO_2 microrods with dominant reactive {010}, {001} facets and nonreactive {101} facets have been prepared by hydrothermal treatment of $Cs_{0.68}Ti_{1.83}O_4/H_{0.68}Ti_{1.83}O_4$ precursor, which displayed a superior photocatalytic performance.[17] Anatase TiO_2 nanocuboids enclosed by active {100} and {001} facets with controllable aspect ratios were solvothermally synthesized by using the titanium tetraisopropoxide as titanium sources and [bmim][BF_4] as the capping agent, which showed extremely high crystalline phase stability and exhibited considerably enhanced photocatalytic activity.[18] Very recently, the rhombic and spindle-shaped anatase nanocrystals with co-exposed {010} and {101} facets, and the rod-like anatase nanocrystals with co-exposed [111]- and {101} facets, and the rutile nanorod composed of lots of highly ordered ultrafine nanowires with co-exposed {110} and {001} facets have been prepared by using the $[Ti_4O_9]^{2-}$ nanosheets as the precursor under hydrothermal conditions, which all exhibited excellent photovoltaic performances than the commercial P25-TiO_2.[19,20] Using similar soft chemical process, the rhombic, tetragonal and leaflike anatase TiO_2 nanocrystals with co-exposed {010}, {001}, and {101} facets have been prepared by using $H_{1.07}Ti_{1.73}O_4$, H_2TiO_3 or $H_2Ti_3O_7$ nanosheets as the precursor, which exhibited excellent photovoltaic performances in dye-sensitized solar cells and enhanced photocatalytic activities for degradation of methylene blue, compared to the commercial P25-TiO_2 nanocrystals.[21–24]

Herein, we demonstrate a facile hydrothermal route for the synthesis of {001}, {010} and {101} facets co-exposed truncated tetragonal bipyramid anatase TiO_2 nanocrystals, and [111]- and {101} facets co-exposed tetragonal cuboid anatase TiO_2 nanocrystals at temperatures from 130 to 180 °C in the presence of HF and H_2O_2. The morphological features, transformed reaction mechanism, and photocatalytic activity of the as-prepared anatase TiO_2 nanocrystals are investigated in detail in this study. Furthermore, compared with commercial P25-TiO_2 nanocrystals, the truncated tetragonal bipyramid and cuboid coexisting of anatase T180-TiO_2 nanocrystals exhibits superior surface photocatalytic activities for the degradation amount of MB per unit surface area of catalyst (mg (MB) per m^2 (TiO_2 surface area)).

2. Experimental section

2.1 Preparation of the $K_2Ti_4O_9$ and $H_2Ti_4O_9 \cdot H_2O$ samples

Potassium tetratitanate ($K_2Ti_4O_9$, KTO) was prepared by a conventional solid-state reaction.[25] Briefly, at first, K_2CO_3 and TiO_2 in a molar ratio of 1.05 : 4 were mixed by ball-milling for 2 h. Then, the mixture was added into an alumina crucible and heated in a muffle furnace at 960 °C for 24 h. 20.0 g of the KTO sample was acid-treated with 2.0 L of 1 mol L^{-1} hydrochloric acid solution at room temperature for 24 h under magnetic stirring to exchange the K^+ with H^+ to obtain the H^+-form of the tetratitanate $H_2Ti_4O_9 \cdot H_2O$ (HTO) sample. The acid treatment was repeated three times to complete the ion-exchange reaction, and then the tetratitanate HTO sample was washed several times with distilled water and dried at room temperature.

2.2 Preparation of TiO_2 nanocrystals

0.5 g of the as-prepared HTO sample was add into a Teflon lined autoclave of 80 mL capacity, and then 50 mL of distilled water, 0.5 mL of HF, and 5 mL of H_2O_2 were added into the above autoclave in order. After the mixture was stirred for 15 min, the autoclave was sealed and the hydrothermal synthesis was conducted in a constant temperature blast drying oven at temperatures from 130 to 180 °C for 24 h. After naturally cooling down to the room temperature, the products were separated from the solution by filtration, and washed several times with distilled water, and then dried at room temperature. The obtained samples were designated as T*x*-TiO_2, where *x* corresponds to the temperature of hydrothermal treatment.

2.3 Sample characterization

The crystalline structure of the samples was determined by powder X-ray diffractometer (XRD, Rigaku MiniFlex II desktop X-ray Diffractometer) with monochromated Cu Kα radiation (λ = 0.15406 nm), operated at 30 kV and 15 mA from 5° to 80° with scanning speed of 8° min^{-1} and step of 0.02°. The surface

morphology of the samples was characterized by scanning electron microscopy (SEM, JSM 7001-F, JEOL, Japan). Transmission electron microscopy (TEM) and selected-area electron diffraction (SAED) were performed using a JEOL Model JEM-2100-F system at 200 kV. Nitrogen adsorption/desorption isotherms were measured at −196 °C on a TriStar II 3020 volumetric adsorption analyzer. Prior to the measurement, the obtained samples were degassed under high vacuum at 120 °C for 5 h. The surface area was calculated from the adsorption isotherm plot in the range of relative pressure from 0.05 to 0.30 by Brunauer–Emmett–Teller (BET) method.

2.4 Photocatalytic experiments

The photocatalytic performance of the TiO_2 nanocrystals was evaluated by the photodegradation of methylene blue (MB, obtained from Beijing Chemical Works) under ultraviolet (UV) light irradiation. 50 mg of the TiO_2 nanocrystals sample was added into a beaker containing 200 mL of MB aqueous solution (2.67×10^{-5} mol L^{-1}) and stirred for 2 h in the darkness to disperse the TiO_2 nanocrystals sample well in the MB aqueous solution and to reach adsorption–desorption equilibrium on the TiO_2 nanocrystals surface. And then the suspension was irradiated by a 175 W ultraviolet lamp with an emission wavelength of 365 nm (Shanghai Mingyao Glass Hardware Tools) under magnetic stirring at room temperature, where the ultraviolet lamp was located 40 cm away from the MB solution surface. At intervals of 20 min, 4 mL of suspension was withdrawn and analyzed after removal of the TiO_2 nanocrystals by using a table-top low speed centrifuge (Jintan Splendor Equipment Manufacture Co. Ltd.). The MB concentration in the solution was determined by using a TU-1901 spectrophotometer (Beijing Purkinje General Instrument Co. Ltd.). The concentration of MB was determined by monitoring the temporal changes in the absorbance maximum at about 650 nm. The photodegradation percentage of MB by the photocatalytic reaction was calculated[26] using the formula $\eta = (C_0 - C_t)/C_0 \times 100\%$, according to the Lambert–Beer law. Where η is the degradation rate, C_0 and C_t represent the initial concentration and the concentration at a certain irradiation time of the MB solution, respectively. As a comparison, the photocatalytic performance of commercially available Degussa P25 TiO_2 (~87% anatase and ~13% rutile phase, obtained from Nippon Aerosil Ltd.) was also measured using the same parameters.

3. Results and discussion

3.1 Characterization of the synthesized KTO, HTO and TiO_2 samples

Fig. 1(a) shows the XRD pattern of the KTO obtained by heating a mixture of K_2CO_3 and TiO_2 at 960 °C for 24 h. All the peaks could be indexed to $K_2Ti_4O_9$ (JCPDS Card File no. 32-0861, space group $C2/m$, $a = 18.186$, $b = 3.774$, $c = 11.962$ Å, $\beta = 106.37°$). The major diffraction peaks at 2θ values of 10.26°, 14.48°, 28.20°, 30.42°, 31.22°, 33.04°, 33.90°, 41.46°, 43.48°, 48.16°, and 52.64° can be indexed to the (200), (201), (310), (311), (004), ($\bar{6}$03), ($\bar{3}$13), (512), (205), (020) and (315) planes of monoclinic structure potassium titanate, respectively, indicating that the KTO phase with a layered structure is successfully obtained. The layered KTO sample has a basal spacing of 8.62 Å that corresponds to the d-value of (200) plane. As shown in Fig. 1(b), after the K^+/H^+ ion-exchange reaction, the HTO sample maintains the same essential layered structure, but the basal spacing changes to 8.82 Å and the diffraction peak of the HTO became weaker and broader than that of the precursor KTO, and the pattern corresponds to JCPDS Card File no. 36-0655 (monoclinic system, space group $C2/m$, $a = 18.77$, $b = 3.72$, $c = 11.62$ Å, $\beta = 104.63°$). Crystallinity of the TiO_2 crystals prepared under various temperatures is analyzed using XRD as shown in Fig. 1(c)–(f). It can be found that the XRD pattern of the obtained crystals displayed diffraction 2θ values at 25.38°, 37.98°, 48.02°, 53.98°, 54.98°, 62.68°, 68.92°, 70.10°, and 75.04°, which corresponds to the (101), (004), (200), (105), (211), (204), (116), (220), and (215) planes of anatase structure of TiO_2, respectively (body-centered tetragonal, $a = b = 3.79$ Å, $c = 9.48$ Å; JCPDS Card File no. 21-1272). No diffraction peaks of any other phases (rutile and brookite) were observed. Therefore, during hydrothermal synthesis process, pure anatase crystals can be obtained at temperatures from 130 to 180 °C. The intensities of the diffraction peaks of the anatase TiO_2 nanocrystals became more intense and sharper with the increase of hydrothermal treatment temperature, implying the increase of crystallinity.

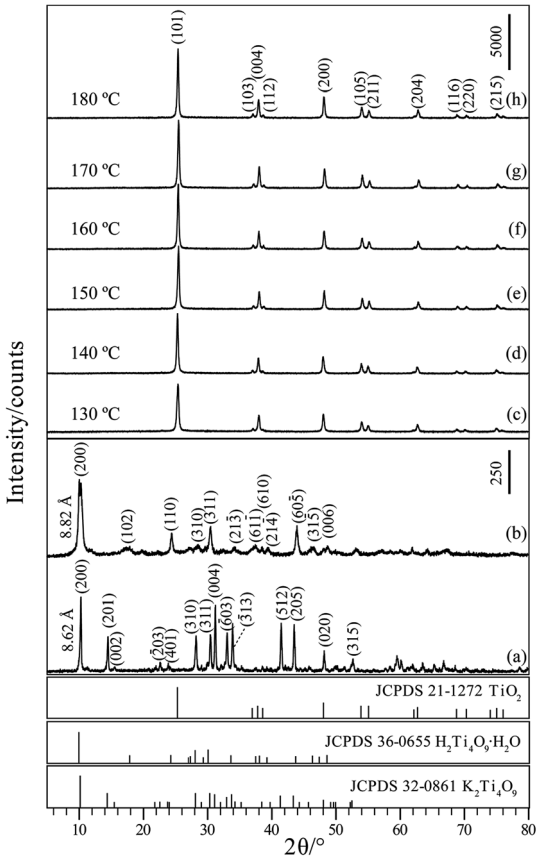

Fig. 1 XRD patterns of (a) $K_2Ti_4O_9$, (b) $H_2Ti_4O_9 \cdot H_2O$, and (c–h) anatase TiO_2 nanocrystals obtained at temperatures from 130 °C to 180 °C.

Fig. 2(a) and (b) shows the SEM images of the KTO and HTO samples, respectively. It can be observed that both KTO and HTO samples exhibit the morphology of nanoribbons. The KTO crystals have a size of 2.5–13.0 μm in length, 260–660 nm in width and 150–300 nm in thickness, and HTO nanoribbons have the size similar to KTO, indicating that the ion-exchange process hardly breaks the shape of the particles. Fig. 2(c)–(n) shows the SEM images of the samples obtained at temperatures from 130 to 180 °C. For T130-TiO_2 sample, the main particles are tetragonal cuboid particles with ~115 nm in length and ~86 nm in width, though some very small irregular particles with the size of a few tens of nanometer were also observed (Fig. 2(c) and (d)). Interestingly, some of tetragonal cuboid particles constitute a nanoribbon secondary particle with ~1.2 μm in length and ~0.3 μm in width. The profile of the secondary particle is very similar to that of the HTO nanoribbons, implying these tetragonal cuboid particles were formed by split the HTO nanoribbons. After hydrothermal treatment at 140 °C, the size of the bigger tetragonal cuboid nanocrystals increased to ~134 nm in length and ~101 nm in width, and the smaller tetragonal cuboid nanocrystals increased to ~58 nm in length and ~50 nm in width and the morphologies also remained (Fig. 2(e) and (f)), indicating the increase of crystallinity. Furthermore, a tiny amount of the truncated tetragonal bipyramid nanocrystals with the length of ~193 nm and the width of ~152 nm were also observed (Fig. 2(e) and (f)). The nanoribbon secondary particles with ~2.8 μm in length and ~0.5 μm in width are polycrystalline particles constructed from the tetragonal cuboid nanocrystals, similar to that of the T130-TiO_2 sample (Fig. 2(c), (e) and (f)). The sample keeps the morphologies of tetragonal cuboid and truncated tetragonal bipyramid when the temperature is above 140 °C, as shown in Fig. 2(g)–(n). High magnification image of the T150-TiO_2, which is shown in Fig. 2(h), illustrates that each truncated tetragonal bipyramid containing the hole on the squared planer crystal facet (*i.e.* {001}-faceted surface) with the width about 65 nm and the depth about 35 nm. The smooth

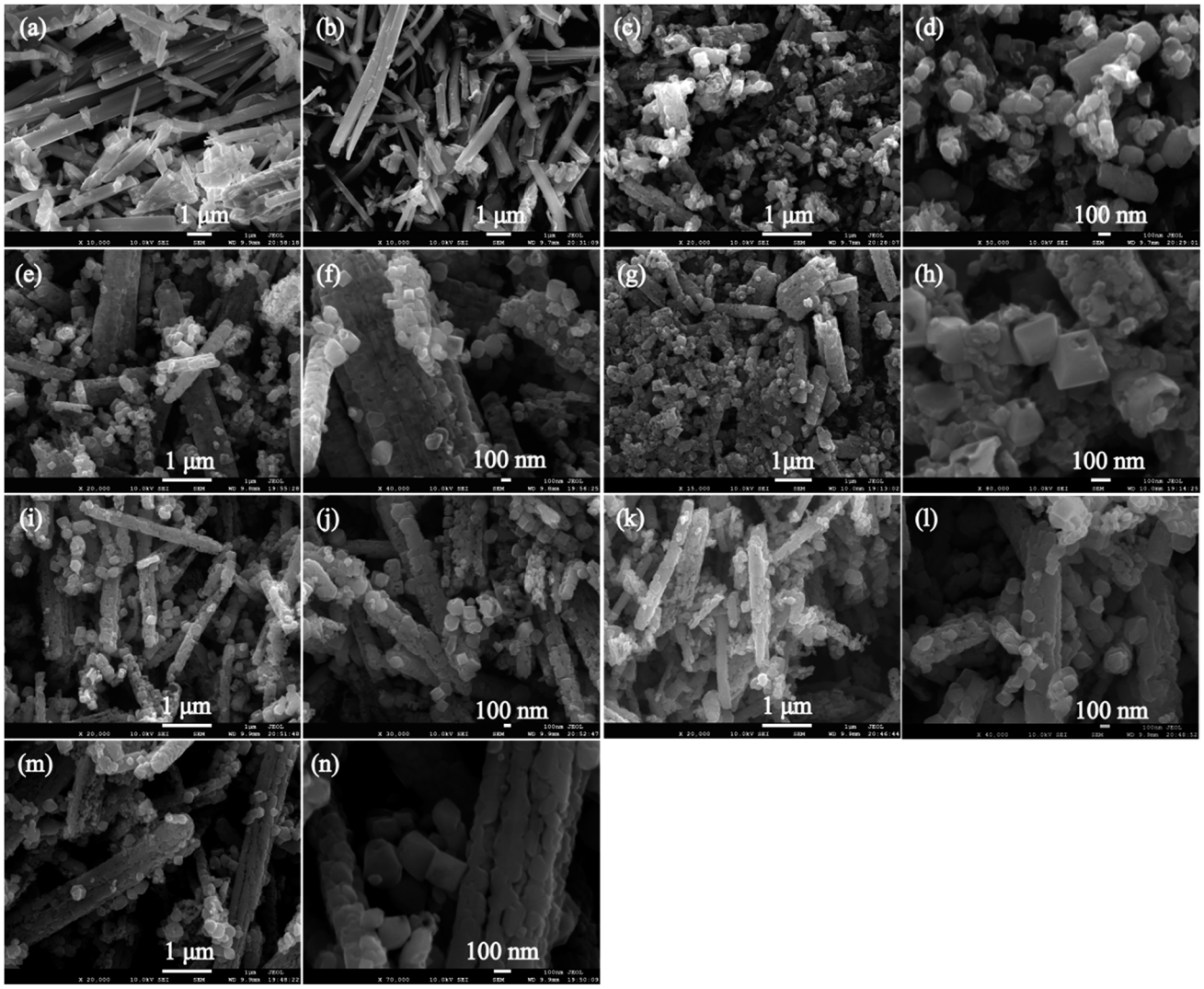

Fig. 2 SEM images of the samples of (a) $K_2Ti_4O_9$, (b) $H_2Ti_4O_9 \cdot H_2O$, (c and d) T130-TiO_2 (anatase phase), (e and f) T140-TiO_2 (anatase phase), (g and h) T150-TiO_2 (anatase phase), (i and j) T160-TiO_2 (anatase phase), (k and l) T170-TiO_2 (anatase phase), and (m and n) T180-TiO_2 (anatase phase).

{001}-faceted surface was eroded away with the hydrothermal process, leading to the formation of hollow single crystals with the remaining eight isosceles trapezoidal {101}-facets surfaces as the frame.[27] This selective etching phenomenon on the {001}-faceted TiO_2 crystal by HF was ascribed to the differences in the geometrical arrangement of oxygen and titanium on {001}- and {101}-faceted surfaces.

TEM images and SAED pattern of T150-TiO_2 further confirm the single-crystalline characteristics (Fig. 3). The truncated tetragonal bipyramid nanocrystals with a size of about 215 nm (Fig. 3(b)), which is consistent with SEM result (Fig. 2(h)). The HRTEM recorded from the white circled area in Fig. 3(b) clearly shows the (101) atomic planes of the truncated tetragonal bipyramid with a lattice spacing of 3.51 Å (Fig. 3(c)), corresponding to the (101) planes of anatase TiO_2 nanocrystals. In addition, the SAED pattern reveals that the truncated tetragonal bipyramid nanocrystal shows a [010]-axis orientation, and the lateral plane of the truncated tetragonal bipyramid nanocrystal corresponds to {010} facet that is vertical to the [010] orientation (Fig. 3(d)). These results demonstrate that the truncated tetragonal bipyramid TiO_2 nanocrystal with {001}, {010} and {101} facets co-exposed on the top/bottom planes, lateral planes, and isosceles trapezoidal planes, respectively.

Fig. 4 shows the TEM, HRTEM images and SAED patterns of T160-TiO_2 nanocrystals synthesized by the hydrothermal process at 160 °C. The TEM images of the sample show tetragonal cuboid TiO_2 nanocrystals with sharp edges and corners and truncated tetragonal bipyramid TiO_2 nanocrystals. Fig. 4(b) shows part of a single tetragonal cuboid TiO_2 nanocrystal with visible lattice fringes. It can be observed that two sets of lattices are present and that they are oriented unperpendicular to each other with an equal lattice spacing of 3.52 Å, corresponding to the (101) and (011) facets of the anatase phase, and the 82° angle between (101) and (011) facets exactly matches the theoretical value 82.1°, calculated from the lattice constants of anatase (tetragonal, space group $I4_1/amd$, JCPDS 21-1272, $Z = 4$, $a = 3.7852$ Å, and $c = 9.5139$ Å).[28] This result reveals that the four lateral planes correspond to {101} facets and the two basal planes correspond to [111]-facets (*i.e.* the crystal is perpendicular to [111] crystal zone axis) of the tetragonal cuboid TiO_2 nanocrystals. It is worth noting that the [111]-facet is different from the {111} facet because the anatase not belongs to a cubic crystal system but belongs to a tetragonal crystal system. Fig. 4(c) and (d) show the magnified TEM image and the corresponding SAED pattern of truncated tetragonal bipyramid nanocrystals obtained at 160 °C, respectively. The yellow dashed lines (Fig. 3(c)) indicate the {001} and {101} crystal planes of the anatase TiO_2 nanocrystal, respectively. The diffraction pattern of bright intense spots indicates that the truncated tetragonal bipyramid TiO_2 nanocrystal is single-crystalline. The angle between different planes ((101) and (114), (101) and (105), (101) and (004), (101) and ($\bar{1}03$)) are designated in Fig. 3(d) agree well the theoretical values.[29] Fig. 4(e) and (f) show the magnified TEM image and the corresponding SAED pattern of tetragonal cuboid TiO_2 nanocrystals obtained at 160 °C, respectively. The yellow dashed lines (Fig. 4(e)) indicate the {101} and {011} crystal planes of the anatase TiO_2 nanocrystal, respectively. The diffraction pattern of bright intense spots indicates that the tetragonal cuboid TiO_2 nanocrystal is also single-crystalline. The angle between different planes ((101) and (011), (101) and (211), (011) and (112), (011) and (110)) are designated in Fig. 4(d) are also consistent with the theoretical values.[29] These results reveal that the two basal planes, the four lateral planes, and the eight isosceles trapezoidal planes of truncated tetragonal bipyramid TiO_2 nanocrystals correspond to {001}, {010}, and {101} facets, respectively; and the four lateral planes and the two basal planes of the tetragonal cuboid TiO_2 nanocrystals correspond to {101} facets and [111]-facets, respectively.

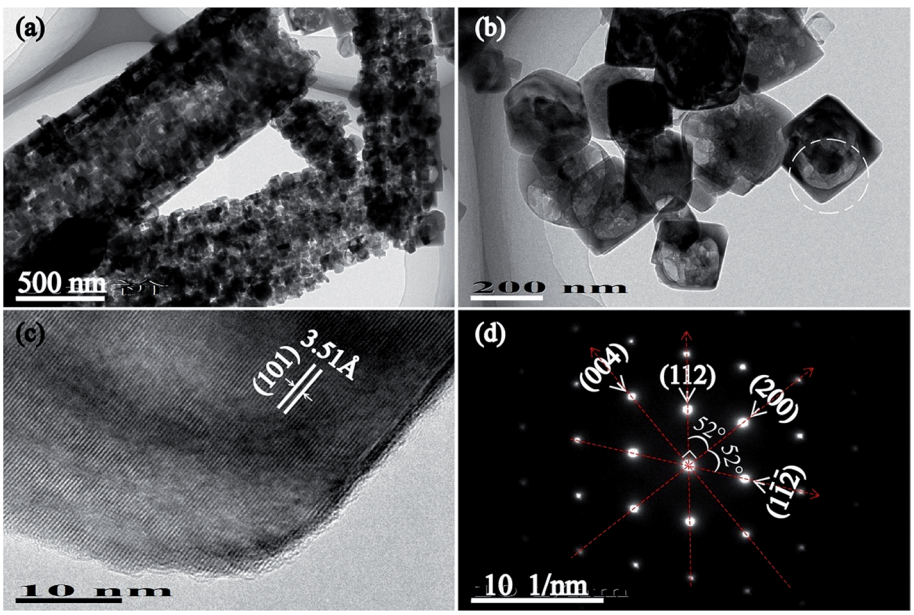

Fig. 3 TEM images (a–c) and the corresponding SAED pattern (d) of T150-TiO_2 (anatase phase).

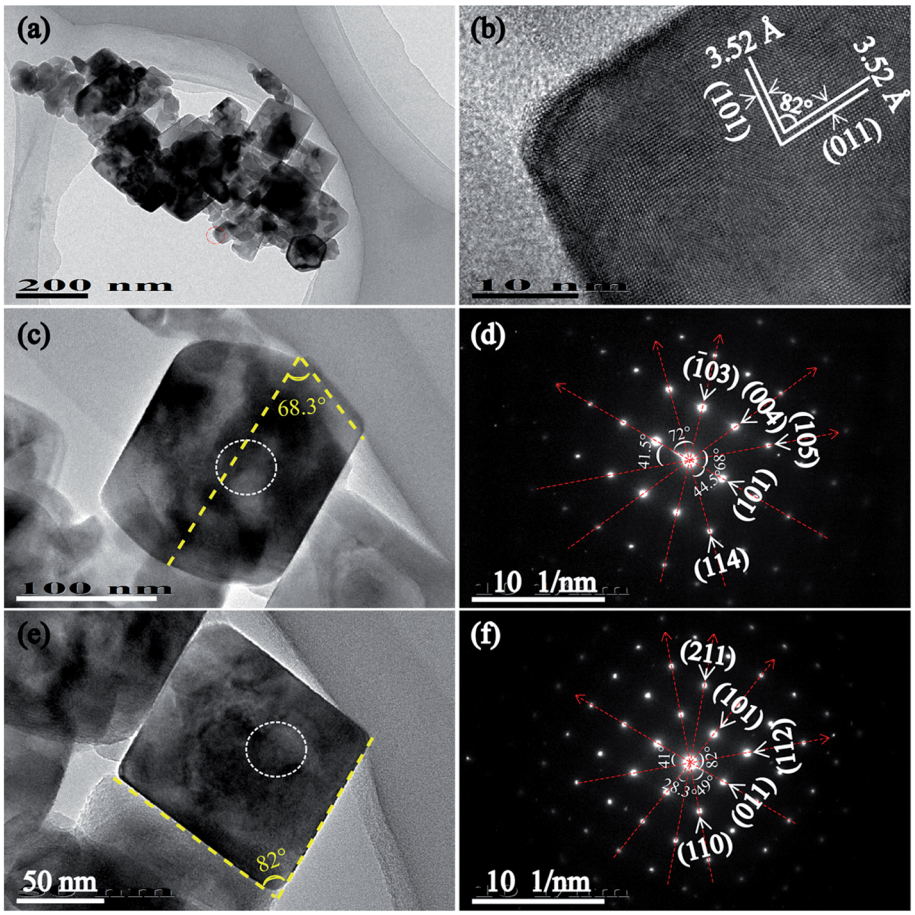

Fig. 4 TEM images (a, b, c, and e) and the corresponding SAED patterns (d and f) of T160-TiO_2 (anatase phase).

Fig. 5(a) is a low TEM image of T170-TiO_2. As the image showed, the nanoribbon particle with ~450 nm in width and several micrometers in length was composed of many nanoparticles, which is accordant with the result of SEM observation (Fig. 2(k) and (l)). Fig. 5(b) is the HRTEM image of the tetragonal cuboid nanocrystal obtained at 170 °C. The interfacial crystal angle between the as marked (101) and (011) crystal planes is 82° which can confirm the exposed crystal facet is [111]-facets. The fast Fourier-transform (FFT) diffraction pattern of the same region (Fig. 5(b) inset) can be indexed to diffraction spots of the [111] zone, which further confirms that the tetragonal cuboid nanocrystal exposed crystal facet is [111]-facets. Fig. 5(c), (d) and (e), (f) are TEM images and the corresponding SAED images of a single tetragonal cuboid nanocrystal and titania nanocube, respectively. According to the analysis above, we can confirm that the exposure of crystal facets are [111]- and {010} facets for the tetragonal cuboid nanocrystal and the titania nanocube, respectively.

Fig. 6(a)–(c) displays the TEM image, HRTEM and the corresponding SAED pattern of the tetragonal cuboid nanocrystals obtained after the hydrothermal treatment at 180 °C for 24 h. It is clear that the tetragonal cuboid nanocrystal displayed two unparalleled lattice fringes of 3.52 Å with the angle of 82°, which can be indexed to the (101) and (011) crystal planes of anatase (Fig. 6(b)). The SAED pattern further confirms that the crystal zone axis of tetragonal cuboid nanocrystal is [111]-direction, that is the exposed [111]-facets on the surface (Fig. 6(c)). The nanoribbon particles are comprise of tetragonal cuboid nanocrystals, nanocube crystals and other irregular morphologies of particles, as shown in Fig. 6(d). For the nanocube crystal, HRTEM image observations reveal three sets of lattice fringes with spacing of 3.52, 3.52, and 3.74 Å, which can be indexed to (101), ($\bar{1}$01), and (002) crystal planes of anatase, respectively. The angles indicated in the HRTEM image are 43.4 and 68.3°, which are identical to the theoretical values obtained from the angles between the (101) and ($\bar{1}$01) crystal planes, and between the (101) and (002) crystal planes of the anatase, respectively (Fig. 6(e)). Therefore, the nanocube crystals preferentially expose the {101} facets on the basal plane. The diffraction pattern of bright intense spots indicates that the irregular TiO_2 nanocrystal is single-crystalline, and the angles between different crystal planes ((101) and (10$\bar{1}$), (101) and (002), (10$\bar{5}$) and ($\bar{1}$05), (200) and (002)) agree well the theoretical values, and the zone axis is indexed to be the [010] direction (Fig. 6(f)).[29]

3.2 Transformation reaction mechanism from tetratitanate HTO to anatase TiO_2 nanocrystals

On the basis of the above discussions, a possible reaction mechanism for the formation of anatase TiO_2 nanocrystals with

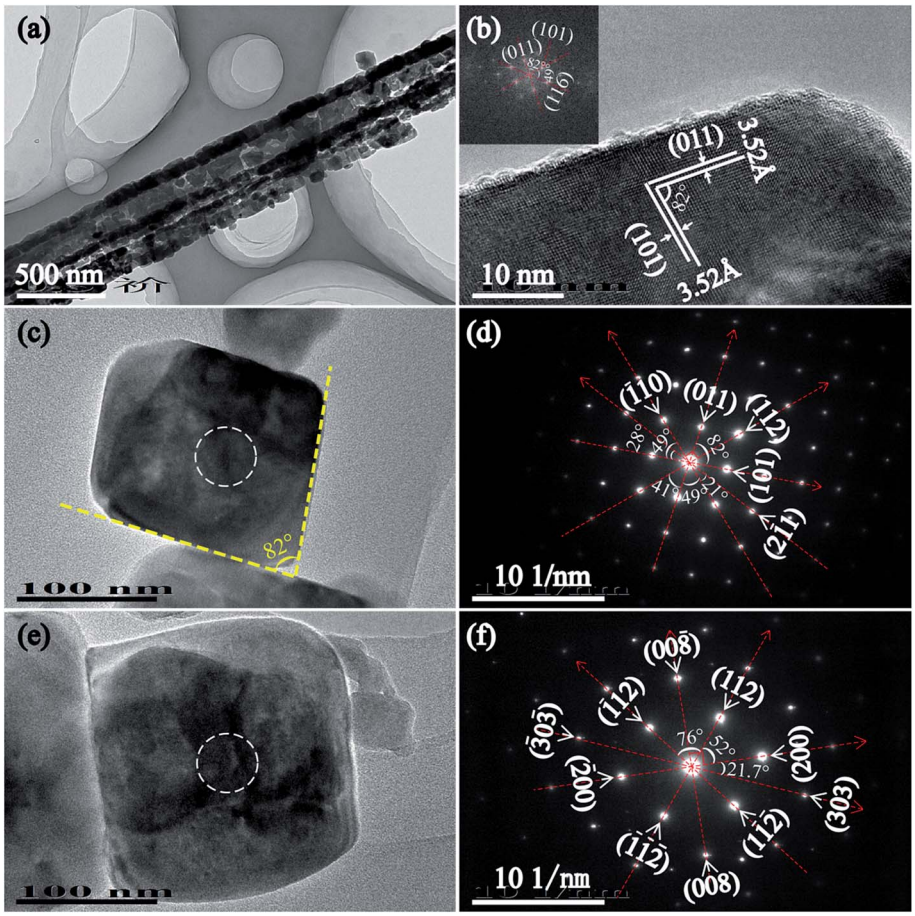

Fig. 5 TEM images (a, b, c, and e), and the corresponding SAED patterns (d and f) of T170-TiO_2 (anatase phase). The inset in the (b) is the fast Fourier-transform (FFT) diffraction pattern.

different morphologies from the tetratitanate HTO precursor in the hydrothermal reaction process is put forward, as shown in Fig. 7. In the HTO crystal structure, the four TiO_6 octahedra are connected with each other *via* edge-sharing at one level to form a structural unit. The structural units are joined to a similar unit above and below by additional edge-sharing to form a 2D zigzag ribbons along the [010] direction, as well as the axial direction of HTO nanoribbons. The zigzag ribbons are connected with each other *via* corner-sharing of TiO_6 octahedra to form a 2D TiO_6 octahedra stepped sheet, which are stacked with a basal spacing of 8.82 Å along the [100] direction (Fig. 1(b)), accommodating H_2O and H_3O^+ (compensates the negative charge of the host sheet) between them.[30] The layered structure of tetratitanate HTO is transformed to the anatase TiO_2 nanocrystals by two types of reactions. One is the *in situ* topotactic transformation reaction, the other is the dissolution–recrystalline reaction, which is similar to the recently reported that the single crystalline anatase TiO_2 nanowires were obtained by the *in situ* transformation and dissolution–precipitation growth from a hydrogen titanate $H_2Ti_2O_5 \cdot H_2O$.[31] In the conversion process of the HTO structure to the anatase structure, first, the HTO structure loses the H_2O molecules in the widely open interlayers of the 2D TiO_6 octahedra stepped sheet. Second, after the interlayer H_2O molecules are totally removed, the monoclinic HTO structure is transformed into tetragonal zigzag ribbonlike anatase structure *via* an *in situ* topotactic dehydration reaction, where the crystal morphology of the nanoribbon precursor is remained after the topotactic reaction.[32] In this reaction, the Ti–O–Ti bonds of the corner-shared by two TiO_6 octahedra are broken along the [010]-direction of the HTO to form H_2O by combining with the H_3O^+ located at the interlayer of the TiO_6 octahedra stepped sheets. The transformation of the stepped sheetlike structure of HTO to the zigzag ribbonlike anatase TiO_2 crystal can be described as follows.

$$[(H_3O^+)_2\,(Ti_4O_9)^{2-}]\cdot H_2O = [(H_3O^+)_2(Ti_4O_9)^{2-}] + H_2O \quad (1)$$

$$[(H_3O^+)_2(Ti_4O_9)^{2-}] = 4TiO_2 + 3H_2O \quad (2)$$

And then, with the proceeding of the hydrothermal reaction, splitting of the ribbonlike anatase TiO_2 crystal in various planes results in the formation of nanoribbon secondary particle with several micrometers in length and hundreds of nanometers in width (Fig. 2). The nanoribbon secondary particle is constructed from lots of small anatase TiO_2 nanocrystals with different morphologies. Namely, the ribbonlike anatase TiO_2 crystal is transformed to anatase TiO_2 nanocrystals mainly *via* the

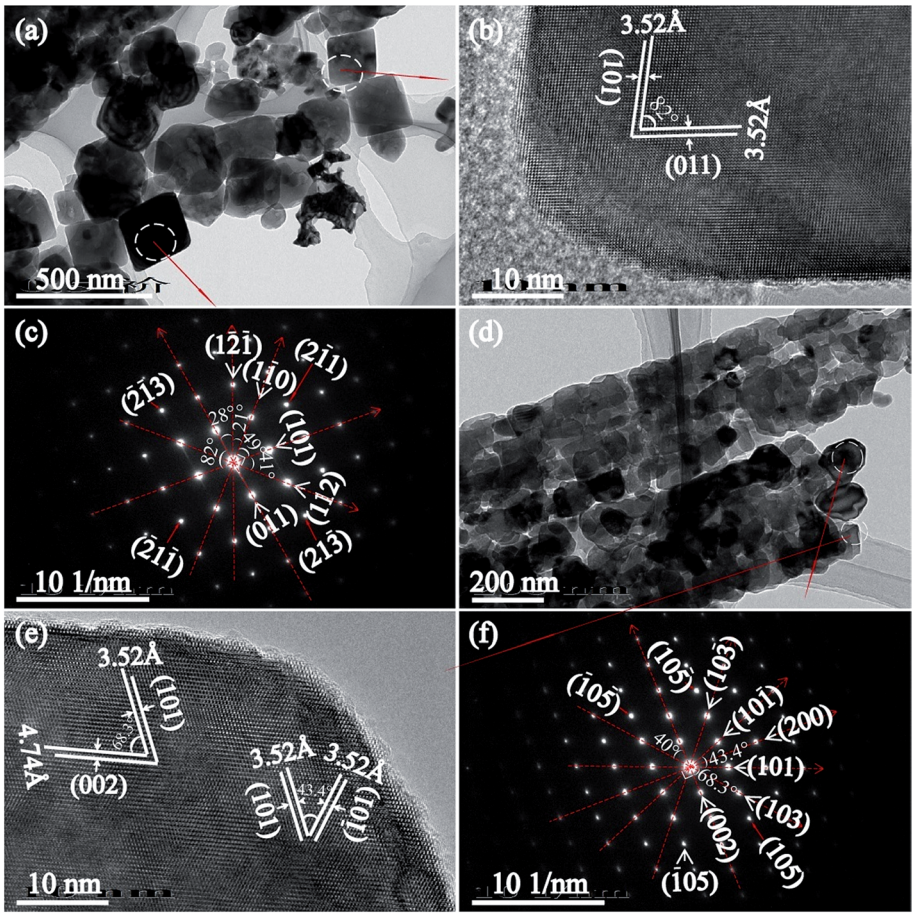

Fig. 6 TEM images (a, b, d, and e), and the corresponding SAED pattern (c and f) of T180-TiO_2 (anatase phase).

dissolution–recrystallization process. The crystal morphologies simulated (on the left in Fig. 7) by using the VESTA software agree well with the SEM images (on the right in Fig. 7). The morphology of truncated tetragonal bipyramid anatase obtained may be explained as due to the splits along (101), (10$\bar{1}$), (001), and (010) planes of the layered structure of the anatase TiO_2. And the truncated tetragonal bipyramid anatase TiO_2 nanocrystal has two basal planes, four lateral planes, and eight isosceles trapezoidal planes, are consistent with the {001}, {010}, and {101} facets, respectively. The corner of 68.3° is consistent with the angle between the (101) and (001) planes. Here, the mixed solution of HF and H_2O_2 plays a significant role in the preparation of anatase TiO_2 nanocrystals with highly reactive {001} facets. HF as a shape-controlling agent can decrease the surface energy of {001} facet to facilitate the growth of {001}-faceted surfaces.[33] Under high concentrations, HF selectively eroded the grown {001}-faceted surface through the following reaction,[34]

$$TiO_2 + 6HF = H_2TiF_6 + 2H_2O \quad (3)$$

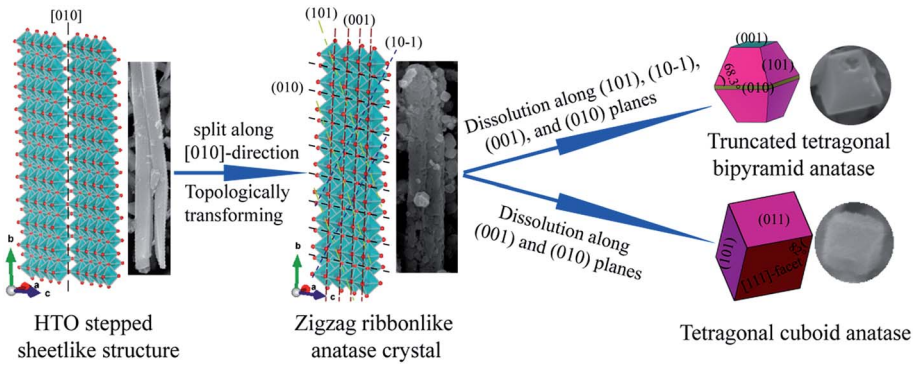

Fig. 7 Transformation reaction mechanism from HTO layered structure to TiO_2 nanocrystals and the simulated crystalline shapes.

When the primary truncated tetragonal bipyramid is eroded by HF to introduce a hole on the {001}-faceted surface. Furthermore, the presence of H_2O_2 is favorable to the formation of anatase single with dominant {001} facets.[35] The F^- ions can efficiency adsorb on the TiO_2 crystal surfaces with the assistance of H_2O_2, resulting in the formation of anatase TiO_2 crystal with dominant {001} facets.[36] The morphology of the tetragonal cuboid anatase obtained may be explained as due to the splits along the (001) and (010) planes of the zigzag ribbonlike anatase crystal during the hydrothermal reaction process, and the formation of the crystal is also accompanied by an Ostwald ripening growth. The tetragonal cuboid anatase TiO_2 nanocrystal formed in the hydrothermal process has two basal planes, and four lateral planes corresponding to the [111]-facets and {101} facets (or {011} facets), respectively. The corner of 82° is consistent with the angle between the (101) and (011) planes.

3.3 Photocatalytic activities

Photocatalytic performances of three typical samples (T150-TiO_2, T170-TiO_2 and T180-TiO_2) with co-exposed high-energy {001}, {010}, and [111]-facets were comparatively evaluated by measuring the photodegradation of methylene blue (MB) aqueous solution under ultraviolet light irradiation, and compared with the commercially available P25-TiO_2 nanocrystals. P25-TiO_2 is a well-known highly active photocatalytic TiO_2 nanocrystals containing 87% anatase phase and 13% rutile phase with an average crystal size about 21.9 nm, where partly of the anatase is the [111]-faceted cuboid nanocrystal, partly of the anatase is the near-spherical nanocrystal without a specific facet on the crystal surface, and a little bit of anatase is the equilateral triangle nanocrystal with {101} facet on one of the lateral planes.[37] Fig. S1† shows the temporal changes in absorption spectra recorded for the P25-TiO_2, T150-TiO_2, T170-TiO_2, T180-TiO_2, and the blank sample under UV irradiation as a function of the irradiation time, respectively. It can be seen from Fig. S1(a)–(d)† that the intensity of the maximal absorption peaks at 665 nm decreased with the extension of irradiation time under UV light irradiation. However, the absorption spectra of the MB does not change for every measurement in the absence of catalyst (Fig. S1(e)†). Hypsochromic effects (*i.e.* blue shifts of spectral bands) were also observed during the course of the photoassisted degradation, implying that the *N*-demethylation of the dimethylamino group in MB occurs concomitantly with oxidative degradation.[38]

The photocatalytic activity of the samples is estimated by the degradation amount of mg (MB) per g (TiO_2), as shown in Fig. 8(a). The degradation amount of MB (mg g^{-1}) increases in the order of without catalyst (0.45 mg) < T180-TiO_2 (21.4 mg) < T170-TiO_2 (22.0 mg) < T150-TiO_2 (22.9 mg) < P25-TiO_2 (23.0 mg), under UV irradiation of 120 min. The commercially available P25-TiO_2 nanocrystals exhibits the high photocatalyst activity in the samples, and T150-TiO_2 shows a relatively high photocatalytic activity in the samples prepared from HTO. It is well known that the specific surface area is an important parameter for the photocatalytic efficiency of the TiO_2 nanocrystals, because the degradation occurs at the surface of the catalyst.[39] The larger specific surface area (S_{BET}) can increase the availability of the active sites for the adsorption of large amounts of organic molecules on the surface and promote the photocatalytic reaction reactions.[40] The S_{BET} of the P25-TiO_2, T150-TiO_2, T170-TiO_2 and T180-TiO_2 was calculated to be 49.7, 15.3, 10.5 and 6.3 $m^2 g^{-1}$, respectively (Fig. S1†). The S_{BET} of P25-TiO_2 is 3.25, 4.73 and 7.89 times higher than that of T150-TiO_2, T170-TiO_2 and T180-TiO_2, respectively. It has been reported that the composite system of anatase/rutile can enhance the photocatalytic activity.[41] Anatase has a little lower conduction band position (0.2 eV) and valence band position (0.39 eV) compared with that of rutile.[42] In the photocatalytic process, the excited electrons can transport from the conduction band position of rutile to that of anatase, while the holes can transport from the valence band position of anatase to that of rutile, which facilitates the efficient electron–hole separation and suppresses the charge recombination, resulting to the enhancement of the photocatalytic activity.[43,44] Therefore, the highest photocatalytic activity of the P25-TiO_2 (containing 87% anatase and 13% rutile) can be attribute to its heterojunction of anatase/rutile and the largest surface area.[45] However, the degradation amount (mg (MB) per g (TiO_2)) for P25-TiO_2 (23.0 mg) is only 1.00, 1.05 and 1.07 times than that of T150-TiO_2 (22.9 mg), T170-TiO_2 (22.0 mg) and T180-TiO_2 (21.4 mg), respectively. The increase times of photocatalytic activity is far less of the increase times of the S_{BET} (Fig. S1†). This result implies that T150-TiO_2, T170-TiO_2 and T180-TiO_2 exhibit higher surface photocatalytic activity than that of P25-TiO_2. To understand the intrinsic photocatalytic activities of the TiO_2 nanocrystals, the degradation amount of MB per unit surface area of catalyst (mg (MB) per m^2 (TiO_2 surface area)) were also investigated, as shown in Fig. 8(b). The degradation amount of MB at 120 min is 0.46, 1.49, 2.09, and 3.90 mg m^{-2} for P25-TiO_2, T150-TiO_2, T170-TiO_2, and T180-TiO_2, respectively. The degradation amount of MB by T180-TiO_2 is 8.48, 2.61 and 1.87 times higher than P25-TiO_2, T150-TiO_2, and T170-TiO_2, respectively. That is, the photocatalytic activity increases in an order of P25-TiO_2 < T150-TiO_2 < T170-TiO_2 < T180-TiO_2.

It is well known that the crystal facets of the TiO_2 nanocrystals are also have an important influence on the photocatalytic activity. It has been reported that the cooperative mechanism of surface atomic structure (the density of under-coordinated Ti atoms) and surface electronic structure (the power of photoexcited charge carriers) plays a decisive role in the enhancement of the photoreactivity. Among the three crystal facets ({101}, {001}, and {010} facets), {001} facet was ever been accounted as the active facets in the photocatalysis because of the higher surface energy (0.90 J m^{-2}) and superior surface atomic structure (100% five-coordinated Ti atoms).[46] However, in view of {010} facet owns both a favorable surface atomic structure (100% five-coordinated Ti atoms) and a higher surface electron structure, the cooperative mechanism existing on {010} facet can improve the electron–hole separation and enhance the photocatalytic activity. Therefore, {010} facet has been considered to be the most active facet in photooxidation reactions for OH radical generation and photoreduction reactions for hydrogen evolution, and the photocatalytic activity

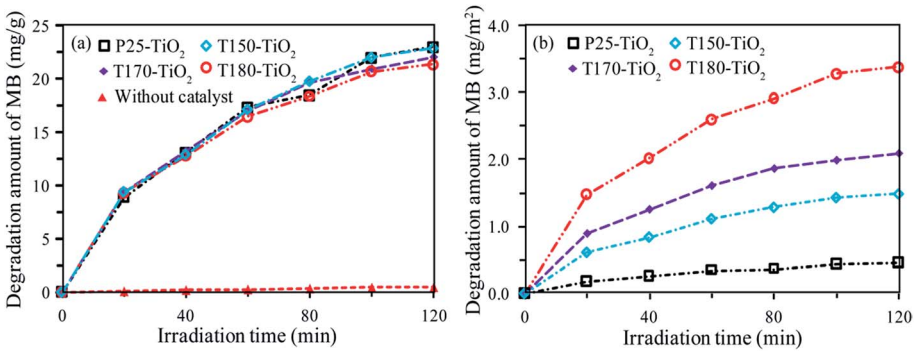

Fig. 8 Photocatalytic degradation amount of 2.67×10^{-5} mol L^{-1} MB aqueous solution in the presence and absence of TiO_2 under UV irradiation presented by (a) mg (MB) per g (TiO_2), and (b) mg (MB) per m^2 (TiO_2), respectively.

increases in an order of {001} < {101} < {010} facets of anatase TiO_2 crystals.[46] Furthermore, in 2013, Xu *et al.* reported that {111} facet also owns both the surface atomic structure (a large percentages of uncoordinated Ti atoms to act as the active reaction sites) and electronic structure (a higher conduction bands minimum to generate more reductive electrons), and TiO_2 single crystals exposed with dominant {111} facet exhibited much higher photocatalytic activity than that of {101}, {001} and {010} facets in the photoreaction to reduce H^+ into H_2.[8] According to our previous discussion, the exposed crystal facets for the T150-TiO_2, T170-TiO_2 and T180-TiO_2 are {001}, {010}, and [111]-facets, and the photocatalytic activity increases in an order of surface without specific facet < [111]-faceted surface < {010}-faceted surface.[19,24] Therefore, the {010} facet may be the most reactive one compared to the {101}, {001} and [111]-facets of anatase TiO_2 crystals. According to the discussion above, the photocatalytic activity increases in an order of P25-TiO_2 < T150-TiO_2 < T170-TiO_2 < T180-TiO_2. This results implies that T180-TiO_2 exhibits the highest surface photocatalytic activity, which can be attributed to the large percentage of co-exposed high-energy {010}, {001}, and [111]-facets.

4. Conclusions

The truncated tetragonal bipyramid anatase TiO_2 nanocrystals with co-exposed {001}, {101} and {010} facets, and the tetragonal cuboid anatase TiO_2 nanocrystals with co-exposed [111]- and {101} facets can be prepared by hydrothermal treatment the layered structure of tetratitanate HTO. The layered structure of tetratitanate HTO is transformed to the anatase TiO_2 nanocrystals by two types of reactions. One is the *in situ* topotactic transformation reaction, the other is the dissolution–recrystalline reaction. First, the stepped sheetlike structure of HTO loses the H_2O molecules in the widely open interlayers. Second, after the interlayer H_2O molecules are totally removed, the monoclinic HTO structure is transformed into tetragonal zigzag ribbonlike anatase structure *via* an *in situ* topotactic dehydration reaction by splitting the Ti–O–Ti bonds of the corner-shared by two TiO_6 octahedra along the [010]-direction of the HTO. And then, during the hydrothermal reaction progress, the zigzag ribbonlike anatase TiO_2 crystals is split into a large amount of anatase TiO_2 nanocrystals with different morphologies by dissolution–recrystalline reaction. The truncated tetragonal bipyramid anatase TiO_2 nanocrystal with co-exposed {001}, {010} and {101} facets on the basal planes, lateral surfaces, and the isosceles trapezoidal planes, respectively, is formed by the dissolution–recrystallization reaction along the (101), (10$\bar{1}$), (001), and (010) planes of the zigzag ribbonlike anatase TiO_2 crystal. The tetragonal cuboid anatase TiO_2 nanocrystal with co-exposed [111]-facets and {101} facets (or {011} facets) is formed by dissolution–recrystallization reaction along the (001) and (010) planes of the zigzag ribbonlike anatase TiO_2 crystal. The truncated tetragonal bipyramid and tetragonal cuboid coexisting of anatase TiO_2 nanocrystals with co-exposed high-energy {001}, {010} and [111]-facets showed high photocatalytic performance for the degradation amount of MB per unit surface area of catalyst (mg (MB) per m^2 (TiO_2 surface area)), compared to that of commercial P25-TiO_2.

Acknowledgements

This work was supported in part by the Grants-in-Aid for Doctor Research Funds from Jinzhong University, the Science and Technology Innovation Project of Shanxi Province Education Department (no. 20121026), the National Science Foundation of China (no. 51272030 and 51572031), and the Grants-in-Aid for Scientific Research (B) (grant number 26289240) from Japan Society for the Promotion of Science and Kagawa University.

Notes and references

1 J. A. Huang, X. Tan, T. Yu, L. Zhao and S. Xue, A Simple and Facile Approach for Synthesis of a Free-Standing TiO_2 Nanotube Layer and Its Photovoltaic Application, *RSC Adv.*, 2012, **2**, 12657–12660.
2 N. Roy, Y. Park, Y. Sohn, K. T. Leung and D. Pradhan, Green Synthesis of Anatase TiO_2 Nanocrystals with Diverse Shapes and their Exposed-Dependent Photoredox Activity, *ACS Appl. Mater. Interfaces*, 2014, **5**, 16498–16507.
3 X. G. Liu and Y. B. Bi, *In Situ* Preparation of Oxygen-Deficient TiO_2 Microspheres with Modified {001} Facets for Enhanced Photocatalytic Activity, *RSC Adv.*, 2017, **7**, 9902–9907.

4 A. C. Parageorgiou, C. L. Pang, Q. Chen and G. Thornton, Low-Dimensional, Reduced Phases of Ultrathin TiO_2, *ACS Nano*, 2007, **1**, 409–414.

5 J. Chen, H. Song, Y. Hou, M. Zhang, M. Jing, X. Jia and X. Ji, Ti^{3+} Self-Doped Dark Rutile TiO_2 Ultrafine Nanorods with Durable High-Rate Capability for Lithium-Ion Batteries, *Adv. Funct. Mater.*, 2015, **25**, 6793–6801.

6 T. Z. Xu, H. Zheng, P. Y. Zhang and W. Lin, Photocatalytic Degradation of a Low Concentration Pharmaceutical Pollutant by Nanoporous TiO_2 Film with Exposed {001} Facets, *RSC Adv.*, 2016, **6**, 95818–95924.

7 P. H. Wen, H. Itoh, W. P. Tang and Q. Feng, Single Nanocrystals of Anatase-Type TiO_2 Prepared from Layered Titanate Nanosheets: Formation Mechanism and Characterization of Surface Properties, *Langmuir*, 2007, **23**, 11782–11790.

8 H. Xu, P. Reunchan, S. X. Ouyang, H. Tong, N. Umezawa, T. Kako and J. H. Ye, Anatase TiO_2 Single Crystals Exposed with High-Reactive {111} Facets Toward Efficient H_2 Evolution, *Chem. Mater.*, 2013, **25**, 405–411.

9 M. Liu, L. Y. Piao, L. Zhao, S. T. Ju, Z. J. Yan, T. He, C. L. Zhou and W. J. Wang, Anatase TiO_2 Single Crystals with Exposed {001} and {110} Facets: Facile Synthesis and Enhanced Photocatalysis, *Chem. Commun.*, 2010, **46**, 1664–1666.

10 H. G. Yang, C. H. Sun, S. Z. Qiao, J. Zou, G. Liu, S. C. Smith, H. M. Cheng and G. Q. Lu, Anatase TiO_2 Single Crystals with a Large Percentage of Reactive Facets, *Nature*, 2008, **453**, 638–642.

11 A. Lazzeri, A. Vittadiniand and A. Selloni, Structure and Energetics of Stoichiometric TiO_2 Anatase Surfaces, *Phys. Rev. B: Condens. Matter Mater. Phys.*, 2001, **63**, 155409.

12 H. G. Yang, G. Liu, S. Z. Qiao, C. H. Sun, Y. G. Jin, S. C. Smith, J. Zou, H. M. Cheng and G. Q. Lu, Solvothermal Synthesis and Photoreactivity of Anatase TiO_2 Nanosheet with Dominant {001} Facets, *J. Am. Chem. Soc.*, 2009, **131**, 4078–4083.

13 J.-M. Wu and M.-L. Tang, Hydrothermal Growth of Nanometer- to Micrometer-Size Anatase Single Crystals with Exposed (001) Facets and Their Ability to Assist Photodegradation of Rhodamine B in Water, *J. Hazard. Mater.*, 2011, **190**, 566–573.

14 J.-M. Wu and M.-L. Tang, One-Pot Synthesis of N-F-Cr-Doped Anatase TiO_2 Microspheres with Nearly All-(011) Surface for Enhanced Solar Adsorption, *Nanoscale*, 2011, **3**, 3915–3922.

15 Q. Y. Li, T. J. Li, S. Z. Chang, Q. S. Tao, B. Z. Tian and J. L. Zhang, Enlarging {110} Exposed Facets of Anatase TiO_2 by the Synergistic Action of Capping Agents, *CrystEngComm*, 2016, **18**, 5074–5078.

16 B. H. Wu, C. Y. Guo, N. F. Zheng, Z. X. Xie and G. D. Stucky, Nonaqueous Production of Nanostructured Anatase with High-Energy Facets, *J. Am. Chem. Soc.*, 2008, **130**, 17563–17567.

17 J. Pan, X. Wu, L. Wang, G. Liu, G. Q. Lu and H. M. Cheng, Synthesis of Anatase TiO_2 Rods with Dominant Reactive {010} Facets for the Photoreduction of CO_2 to CH_4 and Use in Dye-Sensitized Solar Cells, *Chem. Commun.*, 2011, **47**, 8361–8363.

18 X. W. Zhao, W. Z. Jin, J. G. Cai, J. F. Ye, Z. H. Li, Y. R. Ma, J. L. Xie and L. M. Qi, Shape- and Size-Controlled Synthesis of Uniform Anatase TiO_2 Nanocuboids Enclosed by Activity {100} and {001}, *Adv. Funct. Mater.*, 2011, **21**, 3554–3563.

19 Y.-E. Du, Q. Feng, C. D. Chen, Y. Tanaka and X. J. Yang, Photocatalytic and Dye-Sensitized Solar Cell Performances of {010}-Faceted and [111]-Faceted Anatase TiO_2 Nanocrystals Synthesized from Tetratitanate Nanoribbons, *ACS Appl. Mater. Interfaces*, 2014, **6**, 16007–16019.

20 Y.-E. Du, J. Li, Y. F. Liu, X. J. Niu, F. Guo and Q. Feng, Synthesis of {110}-Faceted Rutile TiO_2 Nanocrystals from Tetratitanate Nanoribbons for Improving Dye-Sensitized Solar cell Performances, *RSC Adv.*, 2016, **6**, 9717–9724.

21 C. D. Chen, L. F. Xu, G. A. Sewvandi, T. Kusunose, Y. Tanaka, S. Nakanishi and Q. Feng, Microwave-Assisted Topochemical Conversion of Layered Titanate Nanosheets to {010}-Faceted Anatase Nanocrystal for High Performance Photocatalysts and Dye-Sensitized Solar Cells, *Cryst. Growth Des.*, 2014, **14**, 5801–5811.

22 C. D. Chen, G. A. Sewvandi, T. Kusunose, Y. Tanaka, S. Nakanishi and Q. Feng, Synthesis of {010}-Faceted Anatase TiO_2 Nanoparticles from Layered Nanosheets Titanate for Dye-Sensitized Solar Cells, *CrystEngComm*, 2014, **16**, 8885–8895.

23 C. D. Chen, Y. Ikeuchi, L. F. Xu, G. A. Sewvandi, T. Kusunose, Y. Tanaka, S. Nakanishi, P. H. Wen and Q. Feng, Synthesis of [111]- and {010}-Faceted Anatase TiO_2 Nanocrystals from Trititanate Nanosheets and Their Photocatalytic and DSSC Performances, *Nanosacle*, 2015, **7**, 7980–7981.

24 Y.-E. Du, D. J. Du, Q. Feng and X. J. Yang, Delithiation, Exfoliation and Transformation of Rock-Salt-Structured Li_2TiO_3 to Highly Exposed {010}-Faceted Anatase, *ACS Appl. Mater. Interfaces*, 2015, **7**, 7995–8004.

25 M. He, X. Feng, X. H. Lu, X. Y. Ji, C. Liu, N. Z. Bao and J. Xie, A Controllable Approach for the Synthesis of Titanate Derivatives of Potassium Tetratitanate Fiber, *J. Mater. Sci.*, 2004, **39**, 3745–3750.

26 J.-Y. Zheng, S.-H. Bao, Y. Guo and P. Jin, Anatase TiO_2 Films with Dominant {001} Facets Fabricated by Direct-Current Reactive Magnetron Sputtering at Room Temperature: Oxygen Defects and Enhanced Visible-Light Photocatalytic Behaviors, *ACS Appl. Mater. Interfaces*, 2014, **6**, 5940–5946.

27 Y. Wang, H. M. Zhang, Y. H. Han, P. J. Liu, X. D. Yao and H. J. Zhao, A Selective Etching Phenomenon on {001} Faceted Anatase Titanium Dioxide Sing Crystal Surfaces by Hydrofluoric acid, *Chem. Commun.*, 2011, **47**, 2829–2831.

28 C. J. Howard, T. M. Sabine and F. Dickson, Structural and Thermal Parameters for Rutile and Anatase, *Acta Crystallogr., Sect. B: Struct. Sci.*, 1991, **47**, 462–468.

29 C. K. Nguyen, H. G. Cha and Y. S. Kang, Axis-Oriented, Anatase TiO_2 Single Crystals with Dominant {001} and {100} Facets, *Cryst. Growth Des.*, 2011, **11**, 3947–3953.

30 H. Izawa, S. Klkkawa and M. Kolzuml, Ion Exchange and Dehydration of Layered Titanates, $Na_2Ti_3O_7$ and $K_2Ti_4O_9$, *J. Phys. Chem.*, 1982, **86**, 5023–5026.

31 L.-L. Lai, W. Wen, B. Fu, X.-Y. Qian, J.-B. Liu and J.-M. Wu, Surface Roughening and Top Opening of Single Crystalline

TiO_2 Nanowires for Enhanced Photocatalytic Activity, *Mater. Des.*, 2016, **108**, 581–589.

32 Q. Feng, M. Hirasawa and K. Yanagisawa, Synthesis of Crystal-Axis-Oriented $BaTiO_3$ and Anatase Platelike Particles by a Hydrothermal Soft Chemical Progress, *Chem. Mater.*, 2001, **13**, 290–296.

33 W.-J. Ong, L.-L. Tan, S.-P. Chai, S.-T. Yong and A. R. Mohamed, Highly Reactive {001} Facets of TiO_2-Based Composites: Synthesis, Formation, Mechanism and Characterization, *Nanoscale*, 2014, **6**, 1946–2008.

34 J.-M. Wu, X.-M. Song, L.-Y. Ma and X.-D. Wei, Hydrothermal Growth of Multi-Facet Anatase Spheres, *J. Cryst. Growth*, 2011, **319**, 57–63.

35 T. Y. Li, B. Z. Tian, J. L. Zhang, R. F. Dong, T. T. Wang and F. Yang, Facile Tailoring of Anatase TiO_2 Morphology by Use of H_2O_2: From Microflowers with Dominant {101} Facets to Microspheres with Exposed {001} Facets, *Ind. Eng. Chem. Res.*, 2013, **52**, 6704–6712.

36 M. Liu, H. M. Li, Y. S. Zeng and T. C. Huang, Anatase TiO_2 Single Crystals with Dominant {001} Facets: Facile Fabrication from Ti Powders and Enhanced Photocatalytic Activity, *Appl. Surf. Sci.*, 2013, **274**, 117–123.

37 Y.-E. Du, Y. Bai, Y. F. Liu, Y. Q. Guo, X. M. Cai and Q. Feng, One-Pot Synthesis of [111]-/{010} Facets Coexisting Anatase Nanocrystals with Enhanced Dye-Sensitized Solar Cell Performance, *ChemistrySelect*, 2016, **1**, 6632–6640.

38 T. Y. Zhang, T. Oyama, A. Aoshima, H. Hidaka, J. C. Zhao and N. Serpone, Photooxidative *N*-demethylation of Methylene Blue in Aqueous TiO_2 Dispersions under UV Irradiation, *J. Photochem. Photobiol., A*, 2001, **140**, 163–172.

39 H. M. Zhang, P. R. Liu, F. Li, H. W. Liu, Y. Wang, S. Q. Zhang, M. X. Guo, H. M. Cheng and H. J. Zhao, Facile Fabrication of Anatase TiO_2 Microspheres on Solid Substrates and Surface Crystal Facet Transformation from {001} and {100}, *Chem.–Eur. J.*, 2011, **17**, 5949–5957.

40 O. Carp, C. L. Huisman and A. Reller, Photoinduced Reactivity of Titanium Dioxide, *Prog. Solid State Chem.*, 2004, **32**, 33–177.

41 D. C. Hurum and K. A. Gray, Recombination Pathways in the Degussa P25 Formulation of TiO_2: Surface *versus* Lattice Mechanisms, *J. Phys. Chem. B*, 2005, **109**, 977–980.

42 L. Kavan, M. Gräzel, S. E. Gilbert, C. Klemenz and H. J. Scheel, Electrochemical and Photoelectrochemical Investigation of Single-Crystal Anatase, *J. Am. Chem. Soc.*, 1996, **118**, 6716–6723.

43 D. W. Hu, W. X. Zhang, Y. Tanaka, N. Kusunose, Y. G. Peng and Q. Feng, Mesocrystalline Nanocompositions of TiO_2 Polymorphs: Topochemical Mesocrystal Conversion, Characterization, and Photocatalytic Response, *Cryst. Growth Des.*, 2015, **15**, 1214–1225.

44 D. O. Scanlon, C. W. Dunnill, J. Buckeridge, S. A. Shevlin, A. J. Logsdail, S. M. Woodley, C. R. A. Catlow, M. J. Powell, R. G. Palgrave, I. P. Parkin, G. W. Watson, T. W. Keal, P. Sherwood, A. Walsh and A. A. Sokol, Band Alignment of Rutile and Anatase TiO_2, *Nat. Mater.*, 2013, **12**, 798–801.

45 J. Zhang, Q. Xu, Z. C. Feng, M. J. Li and C. Li, Importance of the Relationship between Surface Phases and Photocatalytic Activity of TiO_2, *Angew. Chem., Int. Ed.*, 2008, **47**, 1766–1769.

46 J. Pan, G. Liu, G. Q. Lu and H. M. Cheng, On the True Photoreactivity Order of {001}, {010}, and {101} Facets of Anatase TiO_2 Crystals, *Angew. Chem., Int. Ed.*, 2011, **50**, 2133–2137.